JURNAL KIMIA VALENSI
p-ISSN: 2460-6065; e-ISSN: 2548-3013
Journal homepage: https://journal.uinjkt.ac.id/index.php/valensi
Research Article

Green Synthesis, Characterization, and Applications of Aluminum Oxide Nanoparticles Using Aqueous Extract of Clove

Waleed Khalid Mahdi[1*], Aqeel Oudah Flayyih[2], Falih Hassan Musa[3]

[1]*Department of Chemistry, College of Education of Pure Science, Ibn–Al Haitham, University of Baghdad, 10053, Iraq*
[2]*Teacher in the Ministry of Education, Baghdad, 10087, Iraq*
[3]*Deputy Dean of the Faculty of Health and Medical Technology, Ashur University, Baghdad, 10053, Iraq*

[*]*Email: waleed.k.m@ihcoedu.uobaghdad.edu.iq*

Article Info
Received: July 20, 2024
Revised: Aug 20, 2024
Accepted: Dec 20, 2024
Online: Dec 25, 2024

Citation:
Mahdi, W. K., Flayyih, A. O., & Musa, F. H. (2024). Green Synthesis, Characterization, and Applications of Aluminum Oxide Nanoparticles Using Aqueous Extract of Clove. *Jurnal Kimia Valensi*, 10(2), 277-289

Doi:
10.15408/jkv.v10i2.40403

Abstract

In this work, γ-Al_2O_3NPs were successfully biosynthesized, mediated aluminum nitrate nona hydrate $Al(NO_3)_3.9H_2O$, sodium hydroxide, and aqueous clove extract in alkali media. The γ-Al_2O_3NPs were characterized by different techniques like Fourier transform infrared spectroscopy (FT-IR), UV-Vis spectroscopy, X-ray diffraction (XRD), scanning electron microscopy (SEM), energy–dispersive x-ray spectroscopy, transmission electron microscope (TEM), Energy-dispersive X-ray spectroscopy (EDX), and atomic force microscopy (AFM). The final results indicated the γ-Al_2O_3NPs nanoparticle size, bonds nature, element phase, crystallinity, morphology, surface image, particle analysis – threshold detection, and the topography parameter. The identified of γ-Al_2O_3 bands were detected by the FT-IR spectroscopy. The UV-visible spectrum of γ -Al_2O_3NPs exhibited an absorption band and (energy gap, Eg = 4.91 eV). It was found that the size range of nanoparticles was (28-37) nm and cubic with agglomerated particles. Antimicrobial activity study showed an excellent inhibition activity of γ-Al_2O_3NPs against *Escherichia coli* negative (G-), *staphylococcus aureus*, positive (G+), and *Candida albicans* fungal. The effectiveness of the adsorption experiment was proven on binary metal ions, such as cobalt, nickel, and copper, by removing them from water using a nanostructured active surface of γ-Al_2O_3NPs. The efficiencies removal of Co^{+2}, Ni^{+2}, and Cu^{+2} ions were 93.22%, 87.49%, and 93.17% respectively.

Keywords: Adsorption, antimicrobial, clove, γ -Al_2O_3 NPs, green synthesis

1. INTRODUCTION

In recent years there are several articles have documented the use of the plant extract for the green synthesis of Al_2O_3NPs for its wide variety of applications, for example, in the field of ceramics, batteries, capacitors, chemical, biological, and defense sensors, as well as in the field of optoelectronics, in addition, to be involved in the manufacture of foodstuffs and textile industries [1]. Green synthesis has attracted significant attention in the research field, leading to the reduction of derivatives, pollution, prevention, and minimization of waste. Green synthesis, which utilizes plant extract to synthesize NPs metal oxide, is non-toxic, environmentally beneficial, and less expensive. It can be employed as a reducing agent during synthesis and has uses in industry, agriculture, medicine, and the environment [2]. In this paper, we used clove, which is a fragrant, dense spice that is an aromatic flower bud of the tree also known as *Syzygium Aromaticum* and is a member of the *Myrtaceae* family order *Myrtales*, *genus*, Kingdom Plantae [3].

This plant is full of antioxidants, including eugenol (phenolic components). The main chemical components of clove oil are phenolic hydroxyl, double bond (C=C), carboxylic acid, and the benzene ring. Also, clove leaves are components of non-phenolic compounds [4]. It is an anti-inflammatory, helping the body fight free radicals that damage cells. It also helps reduce the severity of various diseases such as (diabetes, heart, ulcers, and some types of cancer). In addition, it protects the liver and strengthens its functions. It also protects the stomach from developing ulcers. Scientific research has also proven that eugenol in cloves reduces liver fat or cirrhosis [5].

Alumina Al_2O_3 occurs in two forms: transition or metastable phases Alumina. The metastable phases of Al_2O_3were eta (ŋ), chi (×), theta (θ), kappa (X), gamma (γ), and delta (δ); these phases were related to the biosynthesis methods conditions, temperature, pH, weight et al., α-Al_2O_3 is alumina stable phase [6]. prepared γ-Al_2O_3 from ammonium alum by a recrystallization method [7] , used a novel eco–friendly method to obtain γ-Al_2O_3NPs which have high purity from waste aluminum., synthesized γ-Al_2O_3 NPs by laser ablation of the aluminum target in ethanol with size ranging from 50 to 90 nm [8]. Synthesized $[NiO]_{0.5}$ $[\gamma\text{-}Al_2O_3]_{0.5}$ using the heat treating the spinel NPs at 800 °C to create spinel nanoparticles using liquid-feed flame spray pyrolysis, with an average particle size of 40–60 nm and adorned with Ni metal particles (~ 10 nm in diameter) scattered on the surface, with flowing 5/95 H_2:N_2 100ml /min in a fluidized bed reactor. The supposed activity of the substrates is activated by setting the tone of the developing stimuli [9]. Synthesized γ-Al_2O_3 NPs by using the (sol-gel) technique, and mean diameter = (60 nm) with employing aluminum nitrate nonahydrate, triethanolamine (TEA, NC_2H_5O), and citric acid [10].

γ-Al_2O_3NPs have been synthesized by electrochemical using a rectangular aluminum plate as the anode and an aluminum plate as the cathode [11] , A practical and environmentally friendly method for preparing alumina nanoparticles was inserted using derivative leaves of Calligonum comosum L. The main goal of their study was to treat organic pollutants by evaluating their effectiveness through photocatalysis. The surface morphology analysis also showed that Al_2O_3NPs are crystalline and have crystalline arrangements. Crystalline form. The XRD study showed an average crystal size of 25.1nm, while the band gap value for Al_2O_3NPs was 2.86 eV. These particles have also been shown to be applicable in improving the mechanical performance of vehicles by enhancing the properties of compression and mechanical aerodynamics.

It is important to note that the biosynthesis of nanoparticles using plant extracts instead of conventional chemical methods leads to the formation of highly homogeneous and stable particles in size and shape [12]. The possibility of treating water pollution was highlighted by the research team of Ali and others, who conducted new studies and research linking the relationship between the absorption of cationic dyes and the effect of Al_2O_3NPs on them [13].

Tween-80 and Formamide were used to synthesize gamma-alumina particles, which proved effective in increasing the absorption of methylene blue dye with an increase in the initial concentration from 50 to 400 mg/L and an increase in capacity from 490 to 2210 mg/L at specific conditions (time 10 minutes, pH = 9, and temperature = 60 °C) [14] used the bioreduction approach to synthesize Al_2O_3NPs in the green treatment by using the green synthesis of Al_2O_3NPs with a leaf extract (prunus x Yedoensis) (PYLE). The results showed a reduction of nitrate by (94%) and to enhance the catalytic activity of Al_2O_3NPs, the researchers proposed improving the size of the nanoparticles and the pH to achieve effective and vital medical drugs in a clean environment, so plant extracts were used, such as clove extract for the first time. To synthesize the Al_2O_3NPs which can be used to replace many commercial drugs on the market in addition it has shown effective antimicrobial activities.

The present paper highlights the current scenario and knowledge concerning the capability of clove extract for the eco-benevolent synthesis of γ-Al_2O_3 NPs with particle size (28-32) nm, and also provides optimization strategies and fresh perspective and their impact on the novel preparation of plant extract.

2. MATERIALS AND METHODS

Materials

The materials used are aluminum nitrate nonahydrate $Al(NO_3)_3.9H_2O$ (Merck - GER), sodium hydroxide from (chem alpha- India), EtOH (RBL-pain), $CoSO_4.5H_2O$, $CuSO_4.5H_2O$ and Nickel sulfate heptahydrate ($NiSO_4.7H_2O$). All chemicals are employed without additional purification. Clove (*Syzygium aromaticum*) was taken from a nearby source local market in Baghdad, as shown in **Figure 1(a,b)**.

Preparation of Clove Extract

Cloves must be prepared first by removing contaminants by rinsing them with water and then drying them at 37 °C. Add (20 g) of clove to (200 mL) of deionized water, then heat the mixture for (30 min) with continuous stirring at a temperature of 90 °C. The product will be reddish-purple. It will be cooled to room temperature and then filtered using (Whatman type filter paper), then separated in a tube with a capacity of (1.5 mL using a centrifuge at a speed of (4000 rpm/min) for (15 min) to obtain clove aqueous extract product.

Preparation of γ-Al_2O_3-NPs

7.06 g of $Al(NO_3)_3.9H_2O$ is dissolved in deionized water 30 mL, then add to it an aqueous extract of cloves 100 ml; after that, a drop of 1 M NaOH was added to the mixture with stirring and heating until the value pH = 12, the mixture is left for (48 h) forming a pale green precipitate, then separated

in a centrifuge, washed (with hot deionized water), the operation is returned a second time with (hot ethanol) after that, dried the product in an electric oven at 300 °C for (10 h) to obtain a white powder of γ-Al_2O_3NPs as depicted in **Figure 2**.

(a) (b)

Figure 1. (a) Clove tree, (b) clove (*Syzygium aromaticum*).

Figure 2. The preparation steps of γ- Al_2O_3NP powder using clove extract and aluminum nitrate. Nona hydrate in alkaline media.

Instrumentation techniques

Various approaches were used to synthesize and identify of γ-Al_2O_3NPs. as below: A Balance electronic, Mod/As 220/C/1 kind (RADWAG). Centrifuge (4000–4500) rpm – Centrifuge, Kind PLC.FAITHFUL-Electric oven, model–25AB–kind WHL, (SCL FINETEDI–shaking water bath / kind SCL) at the lab of (Uno-Baghdad-College of edu-Ibn/Al- Hiatham) (Shimadzu-UV-Vis) /(160/UV) spectroscopy. (Shimadzu FT-IRKind -S8500 from (Uno Baghdad / College of Science). XRD/ kind (Holland–XRD-Phillips), from (Baghdad Center/ Lab). (SEM). Type (FE) (Ziess-HV 300 / GER) operating at 10 kV. (EDX). (TEM) 100Kv–Kind GER/ EM10C- 100Kv , at Kashan /Uno - Iran. (AFM) , Kind Liestal - AG nanosurf (Swiss) at (Uno -Baghdad / College of Science). The antimicrobial activity of the synthesized γ-Al_2O_3 NPs was examined with two bacterial strains, (G-), *Escherichia coli* (G+) *Staphylococcus aureus*, and (*Candida Albicans*) fungal (nutrient medium of jellose medium – kind Muller Hinton agar), in a disc using (diffusion method), and (Potato dextrose- PDA – in a nutrient medium) for antifungal activity nutrient. Adsorption measurements were carried out by using (UV-Vis) spectrum type (160/UV) Shimadzu spectroscopy at (Uno - Al-Mustansiriya / College of Science).

Antimicrobial Method

This study shows that two pathogenic bacterial strains are Gram-negative (-ev) and Gram-positive (+ev) bacteria, namely, E. Coli and S. aureus, and Candida albicans fungal. The antimicrobial activity of ammonium oxide nanoparticles was evaluated by the agar diffusion method, using sterile Petri dishes into which nutrient media and seeds of L.B were poured (Loria/Agar Bertani). These clinical isolates are placed in an incubator for a period of (24 h), Separately all these bacterial strains are spread on the agar medium, and a sterile cork drill is used to make a well or wells (6 mm) under sterilization conditions and with special care. In the presence of a Mueller Hinton agar nutrient medium, the disk diffusion method was used to treat Candida albicans fungi. As for measuring the effectiveness of the fungi, the same method of nutrient medium (agar) type (potato dextrose) PDA was used in various concentrations of nanoparticles (i.e., 2,1,0.5, and 0.25

mg/mL) applied to study and evaluate the effectiveness of (γ-Al_2O_3NPs), where these particles are placed in sterile water and dispersed using special high-precision, sterile pipettes, then added to the wells, with a direct test, against pathogens. Then, the dishes are placed in an incubator at 37 °C (36 h). The inhibition zone for each well is then measured, and the results are recorded. The ultimate antimicrobial activity values were estimated in millimeters (mm).

Adsorption Method

Varying selected metal ions solutions with a concentration of 0.00005 gm/mL were made by proper dilution of stock solution, which was agitated for half an hour with pH = 6. This study concluded the effect of the concentrations of (M (II): Co, Ni, Cu) using different metal ions concentrations from 1 to 10 mg /L and 0.5 gm of adsorbent at contact time (1-30) min.

3. RESULTS AND DISCUSSION

An aqueous extract of clove was used with Al $(NO_3)_3.9H_2O$. The changing color solutions are from brown at pH = 6 to peggy at pH = 9, and then to dark brown at pH =12 after adding heating drops of 1 M NaOH. The final product was a white powder of γ-aluminum oxide nanoparticles, as depicted in (**Figures. 3a, b, c, and d**).

Figure 3. Color change of solutions in the alkaline media with $Al(NO_3)_3.9H_2O$ and, bio–redactors of clove extract (a) brown, (b) Peggy, (c) dark brown, and (d) the final product of γ-Al_2O_3 NPs powder.

Characterization

Fourier Transform Infrared (FTIR) of γ-Al_2O_3 NPs

Typically, the FTIR spectrum of γ-Al_2O_3NPs has multiple significant peaks indicative of distinct functional groups within the material. These peaks can reveal information about the structure and chemical composition. Two adsorption bands at (590 and 667cm^{-1}) are among the most noticeable peaks in the FTIR spectra of gamma alumina Nps and were attributed to the stretching vibration mode of Al-O. The peak at 3640 cm^{-1} is due to the stretching vibration of OH. Another peek at 1126 cm^{-1} is due to the CH_2, C-O bond of clove vibrations [15]. Peaks were identified at 543 cm^{-1}, 493 cm^{-1}, and 439 cm^{-1}, which were ascribed to the Al–OH groups' bending vibration [16], as depicted in **Figure 4**.

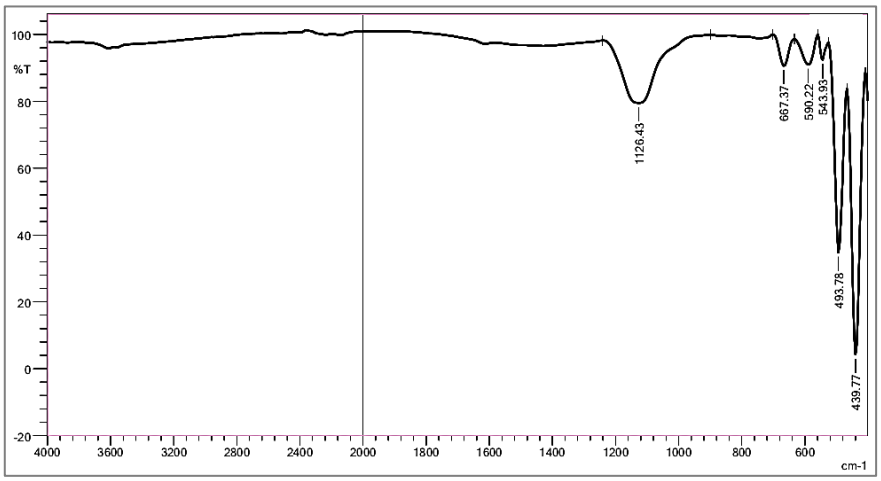

Figure 4. FT-IR of γ - Al_2O_3NPs powder from aqueous clove extract.

UV–Vis spectrum of γ - Al_2O_3 NPs

It has been shown that UV-vis spectroscopy is a reasonably sensitive technique for verifying the synthesis of Al_2O_3-NPs (**Figure 5**). The synthesized Al_2O_3-NP aliquots were examined at different wavelengths between 245 and 500 nm and exposed to UV–visible analysis. According to the literature, the absorption position varies depending on the sources

employed to synthesize Al_2O_3-NPs, such as the seed extract of Phoenix dactylifera (264 nm) [17], the macroalgae Sargassum ilicifolium extract (227 nm) [18], and Citrus aurantium L extract (322 nm) [19]. The UV-vis (Figure .5) showed absorbance peak (λ max) at 252. The energy band gap (Eg) was calculated by 1239.83 / 252 = (4.91 ev) [20].

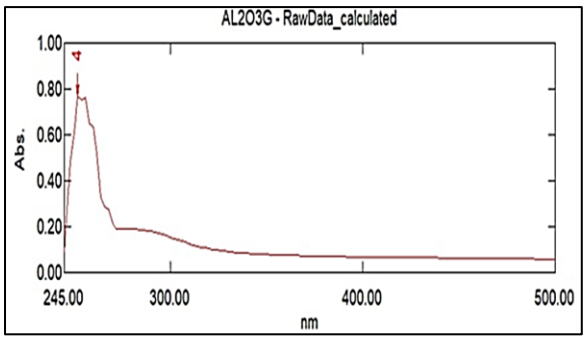

Figure 5. U.V- vis spectrum of γ-Al_2O_3 NPs from aqueous extract of clove.

X-Ray Diffraction (XRD) of γ-Al_2O_3 NPs

Figure 6 illustrates the unique diffraction peaks for γ-Al_2O_3 nanoparticles that are seen at particular 2θ values, indicating that the aluminum oxide nanoparticles are in the single-crystalline phase and belong to the cubic crystal lattice of the aluminum oxide phase, exhibit peaks at 37.70 °, 43.51°, and 63. 06°, which are referred to Miller indices (311), (400), and (440) as shown in **Table 1**. Even so, the existence of broad peaks and additional minors peaks indicates crystallinity and lower phase purity of γ-Al_2O_3 NPs [21], and also the absence of impurity peaks in the XRD spectra underscores the high purity of the γ- Al_2O_3 nanoparticle sample. According to [22], these findings were consistent with (JCPDS card No: 00-029-0063). Debye Scherrer's formula provided an estimate of the crystallite size of around 28.53 nm. :D = K λ / β cos θ,K represents the Scherrer constant (0.9) where λ is the x-ray wavelength, β is full width at half–maximum (FWHM) of the reflections, and θ stands for the Bragg's angle in radian [23]. The average particle size is 35.04 nm, depicted in the XRD data of γ - Al_2O_3 NPs. According to these results, X-ray diffraction was used to determine the crystallite size of Al_2O_3 nanoparticles. The XRD investigation verifies that gamma alumina is present.

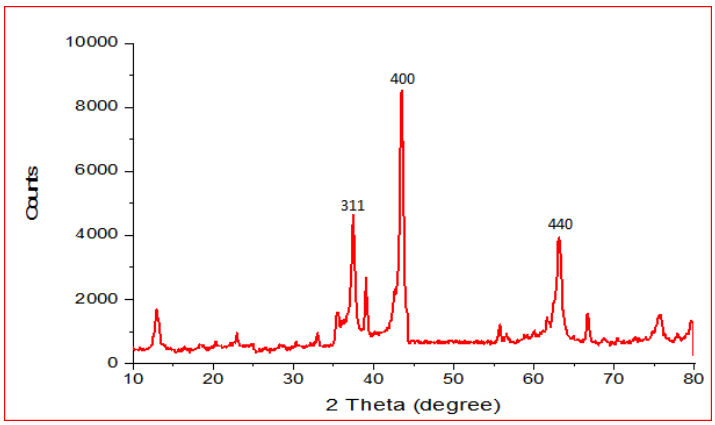

Figure 6. XRD of γ - Al_2O_3 NPs powder from aqueous extract of clove.

Table 1. Represented XRD data of γ-Al_2O_3 NPs

Pos. [° 2Th.]	hkI	FWHM [° 2Th.]	Particle size (nm)	Average particle size
37.4014	311	0.2952	29.69	
43.5194	400	0.3444	25.92	35.04 nm
63.0645	440	0.1968	49.49	

Morphological analysis of γ-Al_2O_3NPs

The nanoparticles' size, shape, and surface characteristics are among the morphological details the SEM may reveal. The form and size of γ-Al_2O_3NPs may be seen by transmission electron microscopy (TEM) images, as depicted in Figures 7(a and b). Different sizes of Np formed ranged from (28 to 37 nm) with agglomerated cubic lattice [24]. The as-prepared nanoparticles' minimal agglomeration nature is evident from TEM investigation, which contributes to their increased surface area and, as a result, their increased antimicrobial activity. One can ascertain the qualities of the material by examining the size and distribution of these particles.

Energy Dispersive X-Ray of γ -Al_2O_3NPs

The EDX results for γ -Al_2O_3NPs are illustrated in **Figure 8**. It was shown that facilitated the γ -Al_2O_3NPs sample elemental composition to be

identified. It was found to consist of A% (35.83% Al and 64.17 % O), confirming the Al_2O_3-NPs structure, that means both Al and O in identical proportions, which indicates that it is chemically pure and compatible with (XRD) [25].

Atomic Force Microscope of γ -Al_2O_3NPs

AFM technique is used to investigate the dispersion and aggregation of NPs with size, shape, and sorption too [26]. **Figure 9** (a,b) and **Table 2**, showed particle (analysis, image), with threshold detection, and information of individual results with global statistics of γ-Al_2O_3NPs powder. The histogram and statistical particle analysis of γ-Al_2O_3NPs are shown in **Figure 10** [27]. The particle analysis's length, height, and width are shown in **Figures 11(a,b). Figures 12 (a,b) and 13 (a, b)** show other particle analysis and topography parameters. The 3D AFM surface structure image of γ-Al_2O_3NPs powder is depicted in **Figure 14** [28].

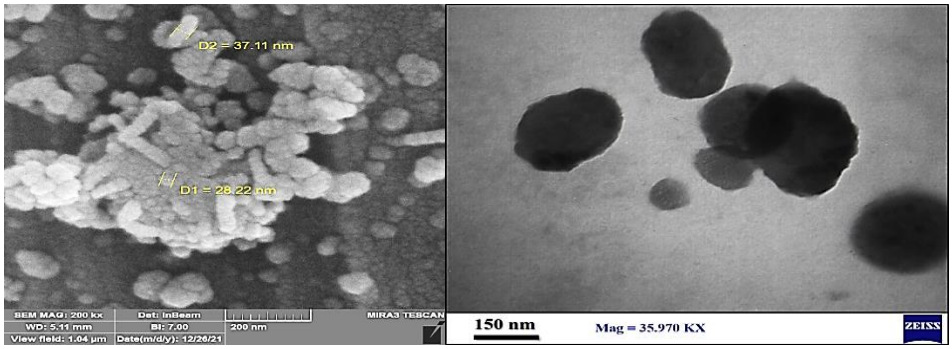

(a) (b)

Figure 7. (a) Images of SEM and (b) TEM of γ-Al_2O_3 NPs powder.

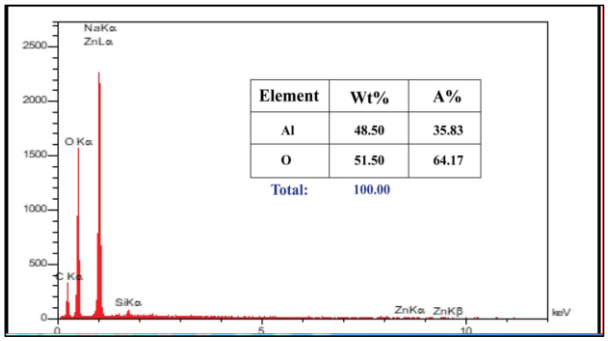

Figure 8. EDX of γ - Al_2O_3 NPs powder from aqueous extract of clove.

Table 2. AFM information and individual results with global statistics of γ- Al_2O_3NPs powder.

Information				
Method 1			Threshold detection	
Threshold 1			1169 nm	
Number of particles			65	
Coverage			21.54 %	
Density			655348 particles / mm2	
Individual results				
Parameters	Project Area	Project Area	Mean diameter	Z-maxim
Unit		Nm^2	nm	nm
Particle N1	small	1525	22.22	1170
Particle N1	small	429.0	16.80	1170
Particle N1	small	5005	65.76	1171
Particle N1	small	3265	54.65	1171
Particle N1	small	3265	54.65	1171
Particle N1	small	4886	67.08	1171
Global Statistics				
Mean		331323	486.2	1190
Min		429.0	16.80	1170
Max		162254	1361	1239

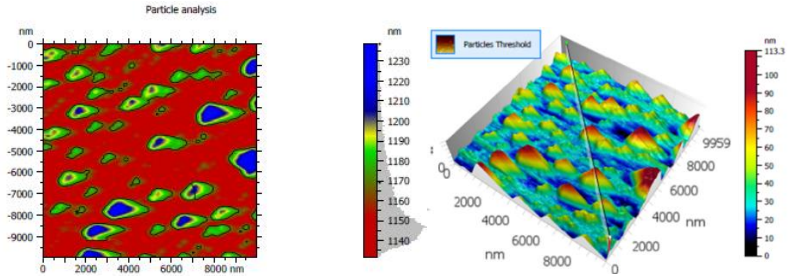

(a) (b)

Figure 9. (a) AFM particle analysis and threshold detection of γ- Al_2O_3NPs powder, (b) Image of particle threshold of γ- Al_2O_3NPs powder

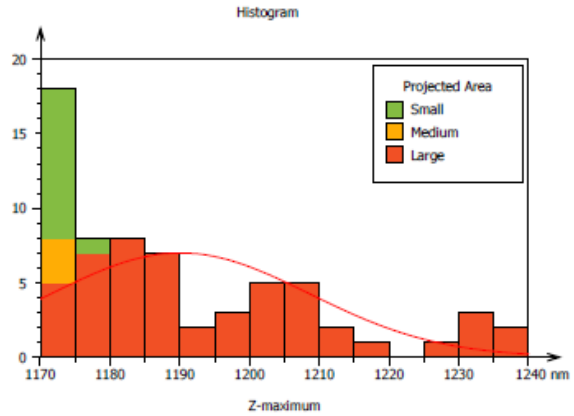

Figure 10. AFM histogram and statistical particle analysis of γ- Al_2O_3NPs powder.

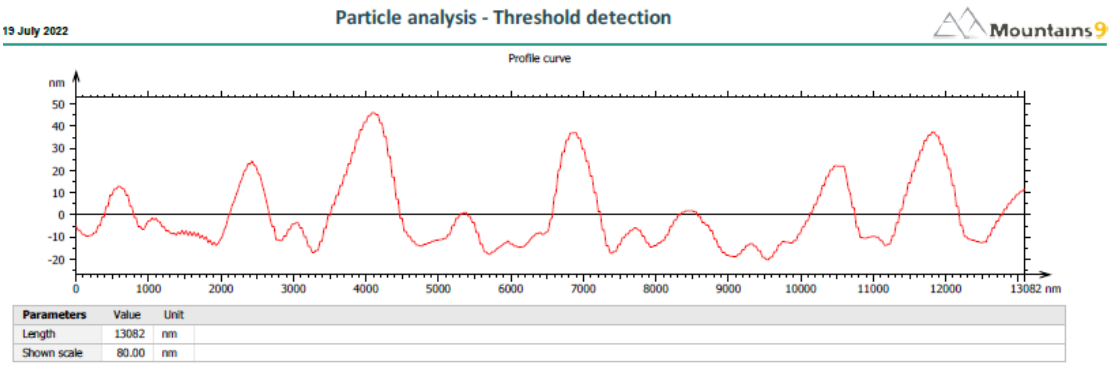

Parameters	Value	Unit
Length	13082	nm
Shown scale	80.00	nm

(a)

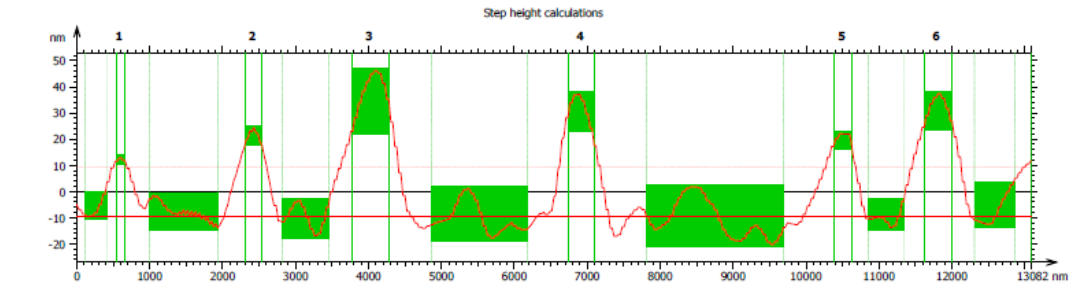

Parameters	Unit	Mean	Min	Max	Step 1	Step 2	Step 3	Step 4	Step 5	Step 6
Width	nm	303.6	110.4	496.8	110.4	220.8	496.8	358.8	248.4	386.4
Maximum height	nm	39.49	22.37	55.60	22.37	33.86	55.60	46.64	31.60	46.90
Mean height	nm	36.00	21.81	48.26	21.81	31.21	48.26	41.90	30.58	42.23

MountainsSPIP® Academic 9.2.9994

(b)

Figure 11. (a) AFM curve of particle analysis length of γ- Al_2O_3NPs powder, (b) AFM height and width calculations parameters of γ- Al_2O_3NPs powder.

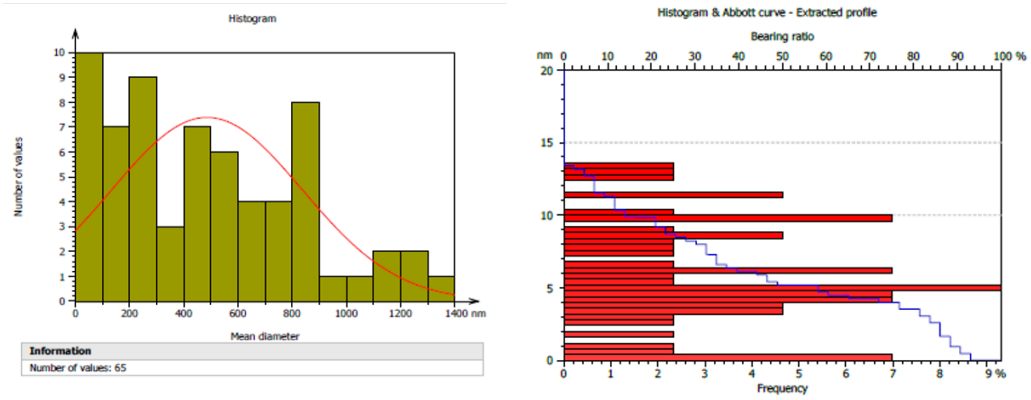

(a) (b)

Figure 12. AFM (a) histogram Number of values against mean diameter, (b) Abbott curve – extracted profile explains the bearing ratio against frequency of γ- Al_2O_3NPs powder.

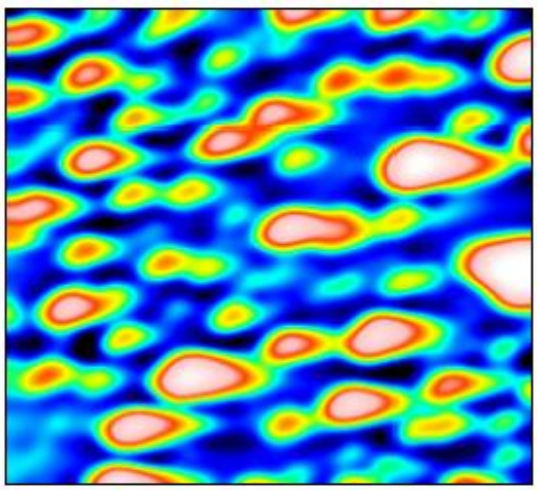

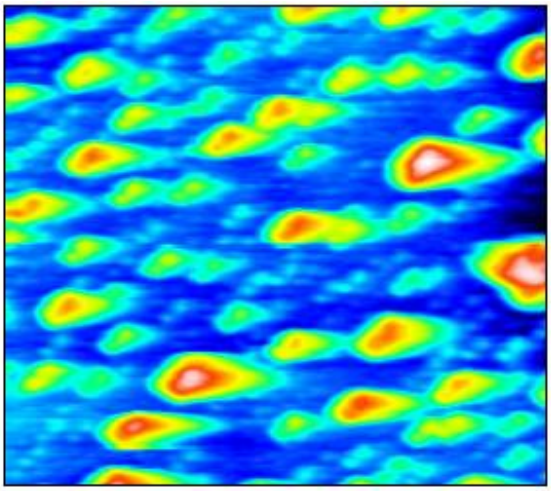

ISO 25178 – Roughness (S-L)			
F: [Workflow] Form removed (LS poly 3)			
S filter (λs): Gaussian, 0.8 µm			
L Filter (λc): Gaussian(order1), 0.0025 µm			
Height parameters			
Sq	13.96	nm	*Root mean square height*
Ssk	2.101		*Skewness*
Sku	8.275		*Kurtosis*
Sp	78.27	nm	*Maximum peak height*
Sv	16.51	nm	*Maximum pit height*
Sz	94.78	nm	*Maximum height*
Sa	10.04	nm	*arithmetical mean height*
Functional parameters			
Smr	100.0	%	*Areal material ratio*
Smc	18.54	nm	*Inverse areal material ratio*
Sdc	29.73	nm	*Material ratio higher difference*
Hybrid parameters			
Sdq	0.0544		*Root mean square gradient*
Sdr	0.1473	%	*Developed interfacial area ratio*

(a)

ISO 25178 – Primary surface			
F: [Workflow] Form removed (LS poly 3)			
F: Leveled (LS), Angle 2.478e10°, 2.609e-10°			
S filter (λs): None			
Height parameters			
Sq	18.17	nm	*Root mean square height*
Ssk	1.347		*Skewness*
Sku	4.580		*Kurtosis*
Sp	81.68	nm	*Maximum peak height*
Sv	31.13	nm	*Maximum pit height*
Sz	112.8	nm	*Maximum height*
Sa	14.21	nm	*arithmetical mean height*
Functional parameters			
Smr	100.0	%	*Areal material ratio*
Smc	26.72	nm	*Inverse areal material ratio*
Sdc	43.38	nm	*Material ratio higher difference*
Hybrid parameters			
Sdq	0.1027		*Root mean square gradient*
Sdr	0.5194	%	*Developed interfacial area ratio*

(b)

Figure 13. AFM images: (a) Roughness (S-L), (b) Primary surface and their topography parameters of γ- Al_2O_3NPs powder.

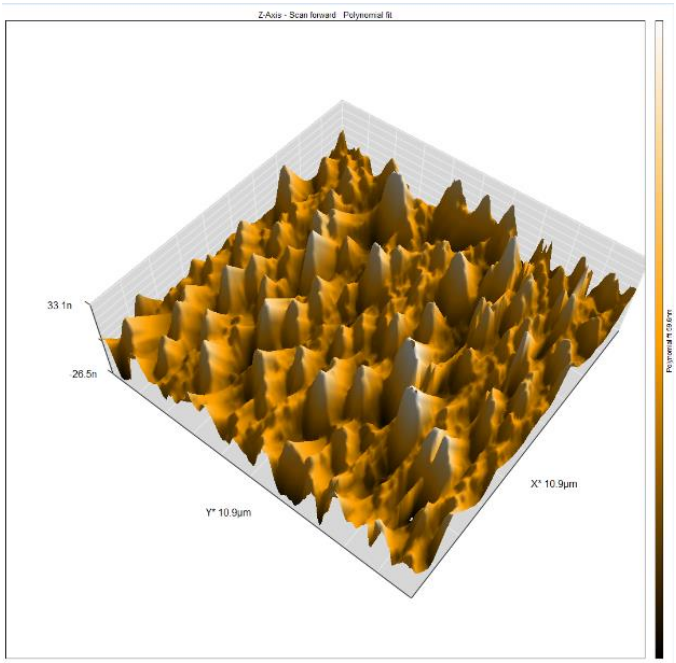

Figure 14. 3D AFM surface structure image of γ- Al_2O_3NPs powder.

Antimicrobial studies

This study used the agar diffusion method to evaluate the antimicrobial activity against *E. coli, S. aureus, E.coli* bacteria, and *Candida albicans* fungi. The results showed that using (diluted hydrochloric acid) or a negative control without using (γ-Al_2O_3NPs) did not show any zone of inhibition. Notably, the antimicrobial *E. Coli* is substantially more prevalent, as depicted in the data below, followed by *C. albicans, S. aureus*, etc. The antimicrobial activity against *C. albicans* is found to range between (20–25) mm; this finding is nearly in agreement with other studies that have been reported [29]. In contrast, the inhibition activity against E. Coli and S. aureus was found to range between (20–31) mm and (15–25) mm at concentrations of (2,1,0.5, and 0.25). On the other hand, the presence of the control alone does not give any effectiveness against bacteria when the leading of γ-Al_2O_3NPs were (2, 1, 0.5, and 0.25) mg /ml.

It was found that at all these concentrations, of γ-Al_2O_3NPs caused a growth delay of all bacteria and Candida albicans fungal as shown in **Table 3** [30]. It showed higher antimicrobial activity at 2 mg /ml for E. coli, while the higher effect in Candida albicans activity occurred at 0.25 mg/mL. The statistical diameter inhibition zones of B samples of γ-Al_2O_3 and the inhibition diameter zones of the antimicrobial of sample (B) in different concentrations are depicted in **Figure 15 (a and b)** [31]. The main mechanisms of realization of the bacteriostatic effect of γ–Al_2O_3NPs are the electrostatic interaction of these nanoparticles with the bacterial outer membrane/cell wall and the formation of aluminum cations initiating the reactive oxygen species (ROS) generation and oxidizing biopolymers.

The direct interaction of Al_2O_3NPs nanoparticles with the exterior membrane surface may be one of the causes of the damage. Therefore, more research is required to validate these findings. Also, the relationship between oxide nanoparticles and the bacterial cell wall and the potential for NP penetration into the bacterial cells remains unclear. Al_2O_3NPs neutralize the bacterial surface charge and form big aggregates because they are considerably smaller than the bacterial cells and coat them with electrostatic attractive forces. Large NP-bacterial complex aggregates would swiftly settle in the suspension.

It suggests a phenomenon that is depending on particle size. While it would be challenging to attract bulk particles, negatively charged bacterial cells (a few micrometers in size) may easily trap NPs through electrostatic attractive forces. In light of the results obtained, we can conclude that the highest effect against bacteria is achieved by γ–Al_2O_3NPs formed from the green synthesis, as depicted in Figure 16 below, where contact between bacteria and nanoparticles results in toxicity to the bacteria and the destruction of diseased cells. It is due to the high antimicrobial activity that has been reported. Finally, γ–Al_2O_3NPs can be used as a powerful antimicrobial agent and treat a wide range of diseases affecting humans.

Table 3. Antimicrobial activity of the γ - Al_2O_3NPs at different concentrations of (B) samples against three pathogenic microbes and their diameter inhibition zoon in (mm).

Samples	B1	B2	B3	B4
Concentrations	2 (mg/mL)	1 (mg/mL)	0.5 (mg/mL)	0.25 (mg/mL)
Microorganisms	Inhibition area diameter in mm for sample (B) γ-Al_2O_3NPs			
Escherichia Coli	31 mm	20 mm	23 mm	25 mm
Staphylococcus aureus	25 mm	21 mm	18 mm	15 mm
Candida albicans	20 mm	25 mm	22 mm	23 mm

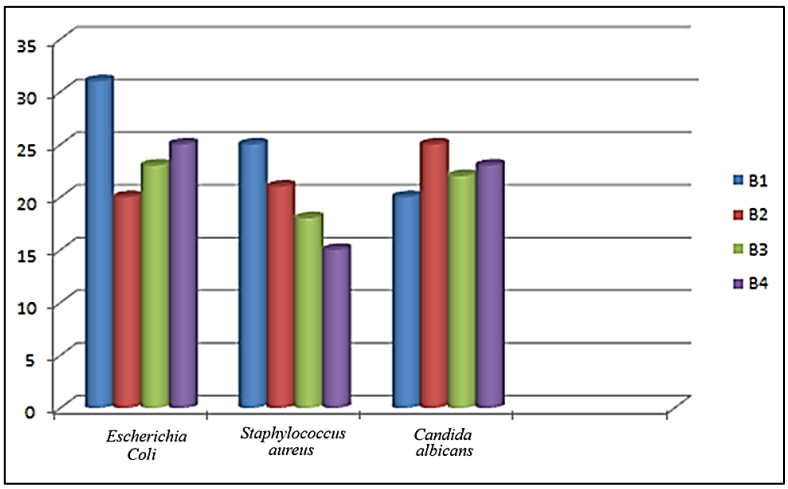

(a)

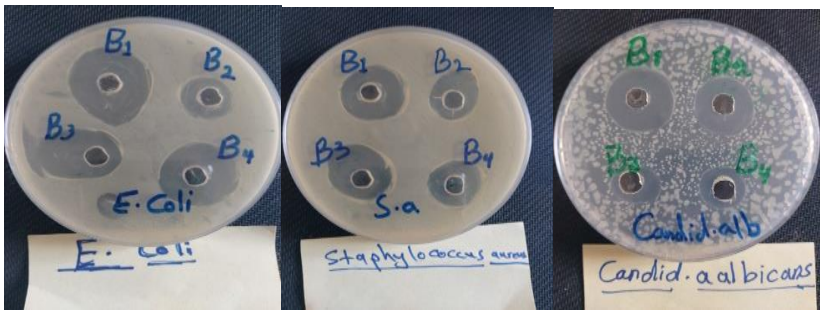

(b)

Figure 15. (a) Statistical diameter inhibition zones in mm of B samples of γ-Al_2O_3 NPs**, (**b) Antimicrobial activity expressed the inhibition of diameter zones of B samples of γ-Al_2O_3NPs at different concentrations against three pathogenic microbes.

Adsorption study

The aim of the biosynthesized of γ-Al_2O_3NPs to generates a good adsorbent for the removal of different divalent metal ions (Cobalt, Nickel, and Copper) from a solution of distilled water was depicted in **Figure 16** [32]. The percentage of cobalt ions removed decreased for γ-Al_2O_3NPs from 95.49 after 10 min to 89.84 after 80 min [33]. In the case of nickel ion removal also decreased from 91.92 after 10 min to 81.08 after 80 min, and the same thing happened from 94.85 to 91.52 for the copper metal ion [34]. The only explanation for that is (γ-Al_2O_3NPs) contain many effective and active sites that prepare for adsorption. When the adsorption process began, these sites were effective. But as time passed, these sites gradually saturated. On this basis, the percentage of displacement efficiency of binary metal ions for each (cobalt, nickel, and copper) is measured was 93.22 %, 87.49 %, and 93.17 %, respectively [35].

The adsorption of Co (II), Ni (II), and Cu (II) ions on the surface of γ-Al_2O_3NPs is based on the interaction of the magnetic attraction between the positive charged of (Co, Ni, and Cu) metal ions and the negatively charged of γ -Al_2O_3NPs by electrostatic forces. Once adsorbed on the surface, the Co (II), Ni (II), and Cu (II) ions can form chemical bonds with surface functional groups such as hydroxyl (-OH) and carboxylate (–COO–) groups [23]. Therefore, heavy ions can be captured from wastewater quickly, so when there is a need to remove pollutants quickly, the

increased adsorption efficiency is of special value and importance, as is the case in conditions where pollutants are in high concentration, so improving and designing systems that have applications such as removing heavy metal ions, wastewater with water purification and environmental treatment depend on such results. Much research deals with improving the practical methods of adsorption techniques and making them more active and effective [36, 37].

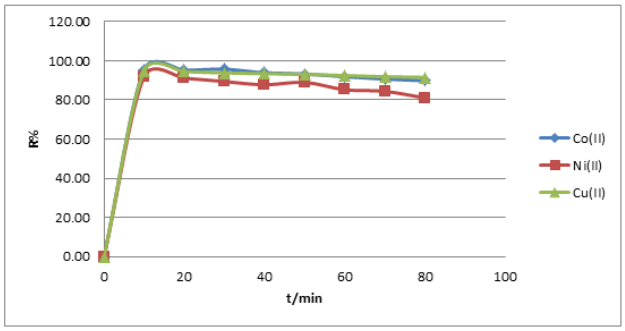

Figure 16. Show the adsorption efficiency curve of some metal ions [Co(II), Ni(II), and Cu (II)].

4. CONCLUSION

γ-Al_2O_3NPs were obtained from the green synthesized method using an aqueous clove extract. Ft-IR exhibited bands at (590 and 667) cm^{-1}, which is attributed to the stretching mode of Al-O. The bands at the range (543-439 cm^{-1}) were due to Al-O, the bending vibration of Al–OH groups. The XRD and the morphology study by SEM & TEM indicate that the aluminum oxide nanoparticles are in the single-crystalline phase and belong to the cubic crystal lattice of the aluminum oxide phase. The structure matched the reference pattern (JCPDS card No:00-029-0063), and the morphology and the size of synthesized γ-Al_2O_3NPs formed particles have different sizes ranging from 28 nm to 37 nm with cubic agglomerated particles. AFM showed particle analysis–threshold detection and the topography parameter.

The measurement of the energy band gap (Eg) mediated UV –vis spectroscopy, which is about 1239.83 / 252 = 4.91ev. EDX revealed the existence of Al and O. It was found that γ –Al_2O_3 was chemically pure. The antimicrobial activity of γ-Al_2O_3NPs was evaluated against *staphylococcus auras*, *E. coli*, and *Candida albicans* fungal when the leading of γ -Al_2O_3NPs were (2, 1, 0.5, and 0.25) mg /ml, it was found that at the higher concentration, the nanoparticles γ-Al_2O_3 caused increasing of the inhibition area diameter of the sample (B) of all bacteria and at the lower concentration gave the same effect on the *Candida albicans* fungal. Adsorption studies show a decrease in the percentage of bioabsorption. The aluminum oxide nanoparticles' active sites are first effective in adsorption; as time goes on, these sites gradually fill and become saturated, decreasing the percentage of adsorbed ions.Co (II), Ni (II), and Cu (II) ions can form chemical bonds with surface functional groups such as hydroxyl (-OH) and carboxylate (–COO–) groups.

The outcome of this work is that the aqueous plant extract clove and monitoring of reaction conditions, temperature, and pH play an important role in enhancing the properties and applications of γ-Al_2O_3NPs. The particle size is a crucial factor in the inhibition activity of bacteria. Also, it contributes to the development of adsorption and increasing their efficiency by removing different kinds of metal ions. That will open the future to researchers for many studies and applications.

ACKNOWLEDGMENT

This work was supported by all authors from Ibn Al-Haitham College of Education for Pure Sciences/Department of Chemistry - University of Baghdad/Iraq, and special thanks to Prof. Dr. Faleh Hassan Mousa from the Department of Medical Laboratory Techniques, Ashur University. Baghdad, Iraq. We also thank all the staff who helped in completing the laboratory analyses.

REFERENCES

1. Tran GT, Nguyen NTH, Nguyen NTT, Nguyen TTT, Nguyen DTC, Tran T Van. Plant extract-mediated synthesis of aluminum oxide nanoparticles for water treatment and biomedical applications: a review. *Environ Chem Lett*. 2023;21(4):2417-2439.
2. Ahmad NM, Mohamed AH, Zainal-Abidin N, Nawahwi MZ, Azzeme AM. Effect of optimisation variable and the role of plant extract in the synthesis of nanoparticles using plant-mediated synthesis approaches. *Inorg Chem Commun*. 2024;161:111839. doi:DOI: 10.1016/j.inoche.2023.111839
3. Otunola GA. Culinary spices in food and medicine: an overview of Syzygium aromaticum (L.) Merr. and LM Perry [Myrtaceae]. *Front Pharmacol*. 2022;12:793200. doi:DOI: 10.3389/fphar.2021.793200
4. Ariswan, Fauzi F, Sumarna, et al. Preliminary results on stability test of clove oil nanoemulsion prepared by ultrasonication process without surfactants. In: *AIP Conference Proceedings*. Vol 2556. AIP Publishing; 2023. doi:10.1063/5.0111227
5. Pandey VK, Srivastava S, Dash KK, et al. Bioactive properties of clove (Syzygium aromaticum) essential oil nanoemulsion: A comprehensive review. *Heliyon*. Published online 2024. doi:https://doi.org/10.1016/j.matchemphys.20

07.02.046
6. Cava S, Tebcherani SM, Souza IA, et al. Structural characterization of phase transition of Al_2O_3 nanopowders obtained by polymeric precursor method. *Mater Chem Phys*. 2007;103(2-3):394-399. doi:https://doi.org/10.1016/j.matchemphys.2007.02.046
7. Baqur MS, Hamied RS, Sukkar KA. An eco-friendly process to produce high-purity nano-γ-Al_2O_3 from aluminum scrap using a novel electrolysis technique for petroleum industry applications. *Arab J Sci Eng*. 2023;48(12):15915-15925. doi:https://doi.org/10.1007/s13369-023-07877-8
8. Wang F, Sun K, Yi E, Laine RM. Chemical modification in and on single phase $[NiO]_{0.5}[Al_2O_3]_{0.5}$ nanopowders produces "chocolate chip-like" $Nix@[NiO]_{0.5-x}[Al_2O_3]_{0.5}$ nanocomposite nanopowders. *J Am Ceram Soc*. 2019;102(12):7145-7153. doi:https://doi.org/10.1111/jace.16632
9. Alamouti AF, Nadafan M, Dehghani Z, Ara MHM, Noghreiyan AV. Structural and optical coefficients investigation of γ-Al_2O_3 nanoparticles using Kramers-Kronig relations and Z–scan technique. *J Asian Ceram Soc*. 2021;9(1):366-373. doi:DOI: 10.1080/21870764.2020.1869881
10. Hussain DH, Rheima AM, Jaber SH. Cadmium ions pollution treatments in aqueous solution using electrochemically synthesized gamma aluminum oxide nanoparticles with DFT study. *Egypt J Chem*. 2020;63(2):417-424. doi:DOI: 10.21608/ejchem.2019.16882.2026
11. Gharbi AH, Laouini SE, Hemmami H, et al. Eco-Friendly Synthesis of Al_2O_3 Nanoparticles: Comprehensive Characterization Properties, Mechanics, and Photocatalytic Dye Adsorption Study. *Coatings*. 2024;14(7):848. doi:DOI: https://doi.org/10.3390/coatings14070848
12. Peralta-Videa JR, Huang Y, Parsons JG, et al. Plant-based green synthesis of metallic nanoparticles: scientific curiosity or a realistic alternative to chemical synthesis? *Nanotechnol Environ Eng*. 2016;1:1-29.
13. Rangasamy P, Hansiya VS, Maheswari PU, Suman T, Geetha N. Phytochemical analysis and evaluation of in vitro antioxidant and anti-urolithiatic potential of various fractions of Clitoria ternatea L. Blue flowered leaves. *Asian J Pharm Anal*. 2019;9(2):67-76. doi:DOI: 10.5958/2231-5675.2019.00014.0
14. Manikandan V, Jayanthi P, Priyadharsan A, Vijayaprathap E, Anbarasan PM, Velmurugan P. Green synthesis of pH-responsive Al_2O_3 nanoparticles: Application to rapid removal of nitrate ions with enhanced antibacterial activity. *J Photochem Photobiol A Chem*. 2019;371:205-215. doi:DOI: https://doi.org/10.1016/j.jphotochem.2018.11.009
15. Tang B, Ge J, Zhuo L, et al. A Facile and Controllable Synthesis of γ-Al_2O_3 Nanostructures without a Surfactant. Published online 2005. doi:https://doi.org/10.1111/j.1551-2916.2009.03005.x
16. Siengchin S, Karger-Kocsis J, Thomann R. Alumina-filled polystyrene micro-and nanocomposites prepared by melt mixing with and without latex precompounding: Structure and properties. *J Appl Polym Sci*. 2007;105(5):2963-2972.
17. Nagarajan P, Subramaniyan V, Elavarasan V, Mohandoss N, Subramaniyan P, Vijayakumar S. Biofabricated aluminium oxide nanoparticles derived from Citrus aurantium L.: antimicrobial, anti-proliferation, and photocatalytic efficiencies. *Sustainability*. 2023;15(2):1743. doi:https://doi.org/10.3390/su15021743
18. Koopi H, Buazar F. A novel one-pot biosynthesis of pure alpha aluminum oxide nanoparticles using the macroalgae Sargassum ilicifolium: a green marine approach. *Ceram Int*. 2018;44(8):8940-8945. doi:https://doi.org/10.1016/j.ceramint.2018.02.091
19. Saleh AK, Shaban AS, Diab MA, Debarnot D, Elzaref AS. Green synthesis and characterization of aluminum oxide nanoparticles using Phoenix dactylifera seed extract along with antimicrobial activity, phytotoxicity, and cytological effects on Vicia faba seeds. *Biomass Convers Biorefinery*. Published online 2023:1-17. doi:https://doi.org/10.1007/s13399-023-04800-x
20. Filatova EO, Konashuk AS. Interpretation of the changing the band gap of Al_2O_3 depending on its crystalline form: connection with different local symmetries. *J Phys Chem C*. 2015;119(35):20755-20761. doi:DOI: 10.1021/acs.jpcc.5b06843
21. Hossein-Zadeh M, Razavi M, Mirzaee O, Ghaderi R. Characterization of properties of Al–Al_2O_3 nano-composite synthesized via milling and subsequent casting. *J King Saud Univ Sci*. 2013;25(1):75-80. doi:DOI: https://doi.org/10.1016/j.jksues.2012.03.001
22. Buwono HP, Adiwidodo S, Wicaksono H,

Firmansyah HI. Hydrothermal synthesis and characterization of nano-particles γ-Al2O3. In: *IOP Conference Series: Materials Science and Engineering*. Vol 1073. IOP Publishing; 2021:12011.

23. El-Sawaf AK, El-Dakkony SR, Zayed MA, et al. Green synthesis and characterization of magnetic gamma alumina nanoparticlesfor copper ions adsorption from synthetic wastewater. *Results Eng*. 2024;22:101971. doi:DOI: https://doi.org/10.1016/j.rineng.2024.101971
24. Atrak K, Ramazani A, Taghavi Fardood S. Green synthesis of amorphous and gamma aluminum oxide nanoparticles by tragacanth gel and comparison of their photocatalytic activity for the degradation of organic dyes. *J Mater Sci Mater Electron*. 2018;29:8347-8353. doi:DOI: https://doi.org/10.1007/s10854-018-8845-2
25. Mohamad SNS, Mahmed N, Halin DSC, Razak KA, Norizan MN, Mohamad IS. Synthesis of alumina nanoparticles by sol-gel method and their applications in the removal of copper ions (Cu^{2+}) from the solution. In: *IOP Conference Series: Materials Science and Engineering*. Vol 701. IOP Publishing; 2019:12034. doi:doi:10.1088/1757-899X/701/1/012034
26. Cascione M, De Matteis V, Persano F, Leporatti S. AFM Characterization of Halloysite clay nanocomposites' superficial properties: current state-of-the-art and perspectives. *Materials (Basel)*. 2022;15(10):3441. doi:DOI: 10.3390/ma15103441
27. Hill D, Barron AR, Alexander S. Controlling the wettability of plastic by thermally embedding coated aluminium oxide nanoparticles into the surface. *J Colloid Interface Sci*. 2020;567:45-53. doi:DOI: https://doi.org/10.1016/j.jcis.2020.01.116
28. Ranjbar M, Dehghan Noudeh G, Hashemipour MA, Mohamadzadeh I. A systematic study and effect of PLA/Al_2O_3 nanoscaffolds as dental resins: Mechanochemical properties. *Artif Cells, Nanomedicine, Biotechnol*. 2019;47(1):201-209. doi:DOI: 10.1080/21691401.2018.1548472
29. Manogar P, Morvinyabesh JE, Ramesh P, et al. Biosynthesis and antimicrobial activity of aluminium oxide nanoparticles using Lyngbya majuscula extract. *Mater Lett*. 2022;311:131569. doi:https://doi.org/10.1016/j.matlet.2021.131569
30. Geoprincy G, Gandhi NN, Renganathan S. Novel antibacterial effects of alumina nanoparticles on Bacillus cereus and Bacillus subtilis in comparison with antibiotics. *Int J Pharm Pharm Sci*. 2012;4:544-548.
31. Ansari MA, Khan HM, Khan AA, Cameotra SS, Alzohairy MA. Anti-biofilm efficacy of silver nanoparticles against MRSA and MRSE isolated from wounds in a tertiary care hospital. *Indian J Med Microbiol*. 2015;33(1):101-109. doi:10.4103/0255-0857.148402
32. Ajibade FO, Adelodun B, Lasisi KH, et al. Environmental pollution and their socioeconomic impacts. In: *Microbe Mediated Remediation of Environmental Contaminants*. Elsevier; 2021:321-354. doi:DOI: 10.1016/B978-0-12-821199-1.00025-0
33. Flayyih AO, Mahdi WK, Zaid YI, Musa FH. Biosynthesis, characterization, and applications of Bismuth oxide nanoparticles using aqueous extract of beta vulgaris. *Chem Methodol*. 2021;6(8):620-628. doi:DOI:10.22034/CHEMM.2022.342124.1522
34. Prochaska C, Gallios G. Nano-adsorbents for cobalt removal from wastewater: a bibliometric analysis of research articles indexed in the Scopus database. *Processes*. 2021;9(7):1177. doi:https://doi.org/10.3390/pr9071177
35. Ali OS, AL-Mammar DE. Adsorption of the Color Pollutant onto NiO Nanoparticles Prepared by a New Green Method. *Iraqi J Sci*. Published online 2024:1824-1838. doi:DOI: https://doi.org/10.24996/ijs.2024.65.4.4
36. Tabesh S, Davar F, Loghman-Estarki MR. Preparation of γ-Al_2O_3 nanoparticles using modified sol-gel method and its use for the adsorption of lead and cadmium ions. *J Alloys Compd*. 2018;730:441-449. doi:https://doi.org/10.1016/j.jallcom.2017.09.246
37. Wuana RA, Okieimen FE. Heavy metals in contaminated soils: a review of sources, chemistry, risks and best available strategies for remediation. *Int Sch Res Not*. 2011;2011(1):402647. doi:https://doi.org/10.5402/2011/402647